3.5 μm mode-locked fiber laser using single-walled carbon nanotube saturable absorber mirror

Jincheng Wei (韦金成)[1#], Peng Li (李鹏)[1#], Linpeng Yu (於林鹏)[1], Shuangchen Ruan (阮双琛)[1,2], Keyi Li (李可意)[1], Peiguang Yan (闫培光)[1], Jiachen Wang (王佳晨)[1], Jinzhang Wang (王金章)[1], Chunyu Guo (郭春雨)[1*], Wenjun Liu (刘文军)[3], Ping Hua (华萍)[4], and Qitao Lue (吕启涛)[5]

[1]Shenzhen Key Laboratory of Laser Engineering, Key Laboratory of Advanced Optical Precision Manufacturing Technology of Guangdong Higher Education Institutes, Guangdong Provincial Key Laboratory of Micro/Nano Optomechatronics Engineering, College of Physics and Optoelectronic Engineering, Shenzhen University, Shenzhen 518060, China

[2]College of New Materials and New Energies, Shenzhen Technology University, Shenzhen 518118, China

[3]State Key Laboratory of Information Photonics and Optical Communications, School of Science, P. O. Box 91, Beijing University of Posts and Telecommunications, Beijing 100876, China

[4]Faculty of Engineering and Physical Sciences, University of Southampton, Southampton SO171BJ, UK

[5]Han's Laser Technology Industry Group Co., Ltd., Shenzhen 518057, China

[#]The authors contribute equally to this paper and should be considered as co-first authors.

*****Corresponding author: cyguo@szu.edu.cn

Received Month X, XXXX; accepted Month X, XXXX; posted online Month X, XXXX

We report on a mid-infrared fiber laser which uses a single-walled carbon nanotube saturable absorber mirror to realize the mode-locking operation. The laser generates 3.5 μm ultra-short pulses from an erbium-doped fluoride fiber by utilizing dual-wavelength pumping scheme. Stable mode-locking is achieved at the 3.5 μm band with a repetition rate of 25.2 MHz. The maximum average power acquired from the laser in the mode-locking regime is 25 mW. The experimental results indicate that carbon nanotube is an effective saturable absorber for mode-locking in the mid-infrared spectral region.

Keywords*:* Mid-infrared laser, fluoride fiber laser, mode-locked laser, saturable absorber.
DOI: 10.3788/COLXXXXXX.XXXXXX.

1. Introduction

In recent years, there is a trend of developing high-performance mid-infrared lasers inspired by their potential applications in spectroscopy, material processing, sensing, defense, and medical surgery [1-3]. Thanks to the progress in the fabrication technique of fluoride fibers (e.g., ZBLAN fibers), rare-earth doped fiber lasers are the most promising mid-infrared sources [4,5]. Various advantages, such as compactness, cost-effectiveness, and high beam quality bestow fiber lasers superiority over solid-state lasers and nonlinear frequency conversion systems that are used for mid-infrared generation previously.

Among mid-infrared sources, the 3.5 μm laser is particularly attractive in spectroscopy and environmental sensing [6], given that the 3.5 μm band covers the absorption peaks of many greenhouse gasses and various volatile organic compounds. An efficient method for generating the 3.5 μm radiation in rare-earth doped fibers is to exploit the $^4F_{9/2}\rightarrow{}^4I_{9/2}$ transition of erbium ions (Er^{3+}). Compared with the 2.8 μm lasers which rely on the $^4I_{11/2}\rightarrow{}^4I_{13/2}$ transition [7-9], the research efforts on the 3.5 μm Er-doped fiber lasers are very limited, due to the lack of appropriate pump sources. Only recently the development of the dual-wavelength pumping (DWP) scheme drives more attention towards the 3.5 μm Er-doped fiber lasers [10,11].

Most applications of the 3.5 μm lasers require the systems to work in pulsed operation modes with high pulse energies and high peak powers [12]. Thus far, a number of 3.5 μm pulsed fiber lasers based upon various mechanisms have been demonstrated. Bawden et al. reported an actively Q-switched Er-doped ZBLAN fiber laser operating at the 3.5 μm band using an acousto-optic modulator (AOM) [13]. Jobin et al. and Luo et al. respectively realized the 3.5 μm gain-switched fiber laser [14,15]. Henderson-Sapir et al. demonstrated a gain-switched 3.5 μm fiber laser using an acousto-optic tunable filter (AOTF) [16].

Compared with the active pulse-generation mechanisms mentioned above, the reports on the 3.5 μm fiber lasers employing passive pulse-generation mechanism are rare. To establish a pulsed operation passively, efficient saturable absorbers (SAs) such as topological materials are desired [17-19]. In recent years, various novel SA materials have been discovered and intensely investigated, and some of them are found to be of excellent performance [20-24]. Unfortunately, the reports on the SAs that can work in the mid-infrared region are rare. At present, only black phosphorus (BP) has been applied successfully to achieve mode-locking and Q-switching in the 3.5 μm region [25,26].

Semiconductor saturable absorber mirror (SESAM) is one of the most popular SAs used in mode-locking and Q-switching, which exhibits strong tolerance to the ambient condition and is easy to realize self-starting. However, the

commercially available InGaAs SESAM can only work efficiently in the spectral region below 3 μm [27]. Another commonly used SA, carbon nanotube (CNT), possesses an operating stability comparable to SESAM [28,29]. Previous works demonstrate that single-walled carbon nanotube (SWCNT) is of outstanding performance in realizing the mode-locking of near-infrared lasers [30-36], and there is a great interest in applying SWCNT to the mid-infrared region. Recently, Wei et al. demonstrated a SWCNT based pulsed lasers operating at 2.8 μm [37], and Chen et al. reported SWCNT based mode-locking in the 2.9 μm spectral region [36]. These works verify the capacity of SWCNT as an effective SA in the mid-infrared region. Compared with BP, SWCNT possesses edge in cost, and the preparation process of SWCNT is easier.

In this paper, we experimentally demonstrate an Er-doped ZBLAN fiber laser mode-locked with a homemade SWCNT saturable absorber mirror (SWCNT-SAM). Stable mode-locking at 3.5 μm is achieved using the laser with a repetition rate of 25.2 MHz. The maximum average power of the mode-locked pulses is 25 mW, corresponding to a pulse energy of 0.98 nJ. To the best of our knowledge, this is the first report on a CNT based mode-locked fiber laser that operates at 3.5 μm. We also observe a Q-switching operation mode in the laser. The results indicate that CNT can play an important role in the realization of 3.5 μm pulsed fiber lasers.

2. Preparation and characterization of SWCNT

The commercially available SWCNT powder is provided by Haolaitech. Co. Ltd.. The powder is prepared via chemical vapor deposition (CVD). We disperse 1 mg SWCNT powder in 1 mL deionized (DI) water. The dispersion is ultra-sonicated at 1.2 kHz under 200 W power for two hours. After the ultra-sonication process, the supernatant (30 μL) of the mixture is transferred onto the surface of a gold-coated mirror using a pipette. The SWCNT-SAM is formed after the DI water is evaporated at room temperature. It should be noted that the uniformity of the generated SAM, in particular the thickness, is limited due to the dropping-based transfer process. However, the concentration of CNTs is generally even, and the SAM exhibits moderate performance as saturable absorber.

Several criteria can be used to explore the characteristics of the homemade SWCNT-SAM. Figure 1(a) shows the as-prepared SWCNT-SAM and the finished dispersion (see inset). The absorption characteristic of SWCNT is related to the diameter of the nanotube. To determine the diameter of the SWCNT fabricated in this work, a transmission electron microscope (TEM, TECNAI G2 F20, FEI. Co.) is used to acquire the images of the sample. As shown in Fig. 1(b) and (c), most SWCNTs are of diameters varying from 1.4 to 2 nm, and a few SWCNTs are of 2.5 nm diameter which matches the 3.5-μm absorption best. Hence, most SWCNTs fabricated by us are not optimized for the absorption of the 3.5 μm radiation, a fact that may be induced by the inappropriate parameters used in the preparation process. Figure 1(d) presents the Raman spectrum measured in the range of 200 to 3000 cm^{-1} with three characteristics (RBM: radial breathing modes, D: disorder mode, and G: tangential mode) [38]. The spectrum confirms that the SWCNT-SAM is clean and free of defects.

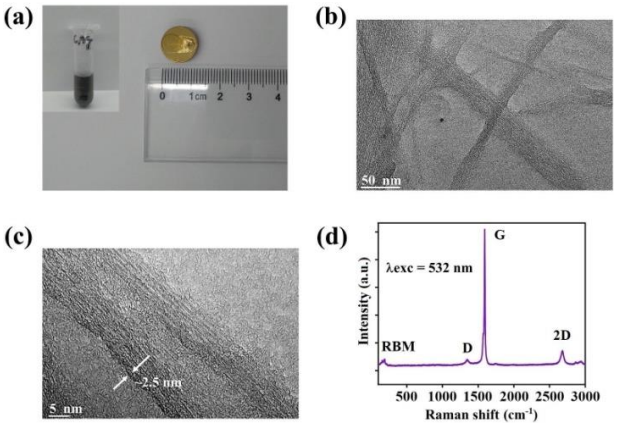

Fig. 1. (a) Prepared SWCNT-SAM. Inset: dispersion of SWCNT. (b) TEM image of SWCNT in coarse resolution. (c) TEM images of SWCNT in fine resolution. (d) Raman spectrum of SWCNT-SAM.

In order to determine the absorption characteristics of the SWCNT-SAM, linear absorption curves are plotted using a Fourier transform infrared spectrometry (VERTEX 80/80V, Bruker). The absorption curves of several areas on the SWCNT-SAM that are of different thicknesses are shown in Fig. 2(a). The corresponding thicknesses of the curves (from top to bottom) are respectively 410 nm, 660 nm, 963 nm and 1010 nm. It should be noted that the concentrations of CNTs in the four areas are generally equal. It also should be noted that in the experimental works, the areas with the CNT layer thicknesses of 410 nm and 660 nm cannot support mode-locking operation, whereas mode-locking can be activated in the other two areas.

Regarding the characterization of the nonlinear absorption of the SWCNT-SAM, a conventional approach involving a dual-arm detection scheme is used. A 3.5 μm optical parametric amplification (OPA) system (ORPHEUS-ONE-HP, Light Conversion) with a repetition rate of 520.8 kHz and a maximum average output power of 1.3 W is employed as the light source. The pulse duration of the OPA's output is several hundreds of femtosecends. The output of the OPA is first sent through a tunable attenuator and then split into two beams by a dichroic mirror (splitting ratio: 50/50). The reflected beam is directly received by a power meter for monitoring the fluctuation of the intensity.

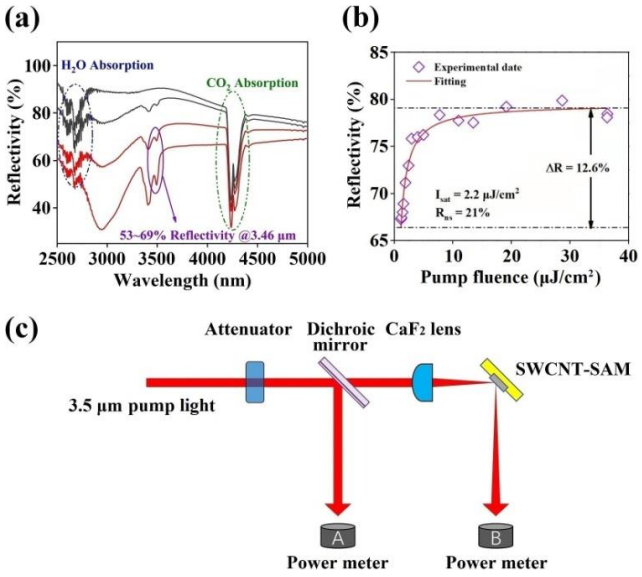

Fig. 2. Linear (a) and nonlinear (b) reflection characteristics of SWCNT-SAM. (c) Schematic of the setup for characterizing saturable absorption.

The transmitted beam is focused onto the SWCNT-SAM using a CaF_2 plano-convex lens, and then reflected, and finally received by another power meter. The saturable absorption curve and the schematic of the measurement setup are presented in Fig. 2(b) and (c). The curve (in a form of the reflectivity of the SWCNT-SAM) is fitted by a simple model:

$$R(I) = 1 - \Delta R \exp(-\frac{I}{I_{sat}}) - R_{ns} \quad (1)$$

from which the modulation depth ΔR is determined to be 12.6%. The non-saturable loss R_{ns} and the saturated fluence I_{sat} are determined as 21% and 2.2 μJ/cm², respectively. These values can be compared with the nonlinear absorption characteristics of SWCNT in the 2.8 μm region reported by Chen et al. [36], in which the modulation depth and non-saturable loss are 16.5% and 71.8%, respectively. It should be noted that although the recovery time of CNT is ~1 ps, the realized pulse duration can be much shorter than that [39].

3. Experimental setup

The experimental setup of the 3.5 μm mode-locked Er-doped ZBLAN fiber laser is presented in Fig. 3. The DWP scheme utilizes two pump sources with wavelengths at 976 nm and 1973 nm, respectively. The 976 nm pump is a commercial laser diode (LD). The 1973 nm pump is an in-house built thulium doped fiber laser, of which the wavelength is determined according to the energy gap between the $^4I_{11/2}$ and $^4F_{9/2}$ energy level of Er^{3+} in ZBLAN host (~5070 cm^{-1}). The beams of the 976 nm pump and the 1973 nm pump are collimated by two lenses: L1 (LA1540, Thorlabs) and L2 (LA1540, Thorlabs), and then combined with a dichroic mirror (DM1, DMSP1550, Thorlabs). The combined pump radiation is coupled into a 4.2-meter-long double-cladding Er-doped ZBLAN fiber (Le Verre Fluoré, core/cladding diameter: 16.5/240, core/cladding NA: 0.125/0.4) using the L3 lens (LA5315, Thorlabs). The generated signal laser and the unabsorbed pump are sent out from the other end of the fiber which is angularly cleaved to eliminate Fresnel reflection. The tips of the fiber are not protected using end caps, given that the humidity of the environment is well controlled and that the laser is operating under low power. Failure of fiber tips is not observed throughout the experimental works. We use an off-axis parabolic mirror (MPD00M9-M03, Thorlabs) instead of a lens to collimate the output, for reducing the absorption loss. Two parallel placed dichroic mirrors, DM4 and DM5, which are of a high reflectivity at 3.5 μm (R > 99%) and a high transmittance at 976 nm (T > 86%) and 1973 nm (T > 91%) are used to separate the 3.5 μm signal from the unabsorbed pump. The signal is focused onto the SWCNT-SAM using the L4 lens. The output port of the laser is performed by a dichroic mirror, DM3, which is of an 85 % reflectivity at 3.5 μm and a high transmittance at the wavelengths of the pump radiations. DM3 is in butt coupling with the ZBLAN fiber. Another dichroic mirror, DM2, which is of the identical spectral performance with DM4 and DM5, is used to guide the signal beam out of the cavity of the laser. Finally, a bandpass filter (FB3500-500, Thorlabs) is employed to further strip the residual pump and amplified spontaneous emission (ASE) from the 3.5 μm signal before the signal is received by the measurement devices. The total dispersion of the laser cavity at 3.5 μm is ~–0.7 ps^2, which is calculated from the dispersion parameter of the ZBLAN fiber (~26.5 ps nm^{-1} km^{-1}). It should be noted that the entire setup is in direct contact with the ambient air. No damage of the fiber or the optical elements is observed during the experimental works, in view of that the humidity and the temperature of the environment are carefully controlled.

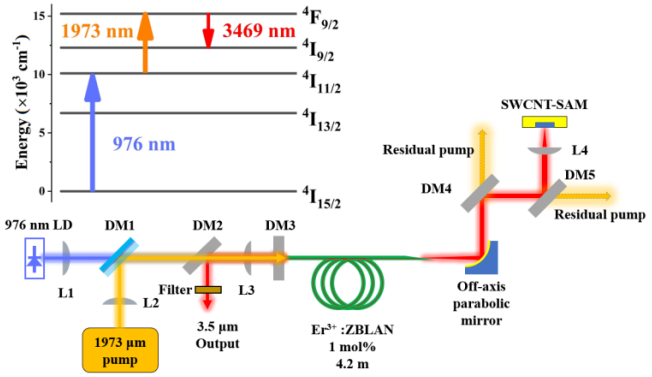

Fig. 3. Experimental setup of the 3.5 μm mode-locked fiber laser, and the diagram showing the transition processes involved in the generation of the 3.5 μm radiation.

4. Experimental results

We first use a gold-coated mirror to replace the SWCNT-SAM, and establish CW lasing with the setup for optimizing the alignment of the optical elements. After the alignment of the elements is optimized, the SWCNT-SAM is placed into the setup. The laser beam is carefully focused onto the surface of the SWCNT-SAM. Mode-locking at 3.5 μm is established by raising the pump power. A maximum output power of 25 mW for the mode-locking operation is achieved as the powers of the 976 nm pump and the 1973 nm pump are tuned to 6.5 W and 2.7 W, respectively. The diameter of the laser spot on the surface of the SWCNT-SAM is ~22 μm. The intracavity power of the laser during operation can be estimated as 167 mW, based upon the output power (25 mW) and the output coupling ratio of the laser cavity (15%). Given that almost all intracavity power is received by the SWCNT-SAM, we estimate the intensity of the laser beam focused on the SWCNT-SAM to be ~0.044 MW/cm^2, which is lower than the saturation intensity of the SWCNT (2 MW/cm^2). The output characteristics of the laser are acquired using the following equipments: optical spectrum analyzer (OSA207C, Thorlabs), oscilloscope (SDA 820Zi-B, Teledyne Lecroy, bandwidth: 20 GHz), radio frequency (RF) spectrum analyzer (N9320A, Agilent), and photodetector (PCI-9, VIGO System, bandwidth: 250 MHz).

The spectrum of the mode-locked laser is presented in Fig. 4(a). The central wavelength of the laser locates at 3470 nm. The full width at half maximum (FWHM) of the spectrum is 7.6 nm. Sharp spikes are observed in the spectrum. However, the essence of the spikes cannot be determined. The locations of the spikes exhibit significant disagreement with the locations of Kelly sidebands calculated using the method developed by Dennis et al. [40]. The wavelength of Kelly sideband is governed by the following equation:

$$\frac{\Delta\lambda_N^{\ 2}}{N} = \frac{2\lambda_0^{\ 2}}{cDL} \qquad (2)$$

in which N represents the sideband order, $\Delta\lambda_N$ represents the wavelength offset from the central wavelength for the N-th order sideband, λ_0 represents the central wavelength of the pulse, c represents the speed of light, D represents the fiber dispersion parameter, and L represents the fiber length. In this case, the values of λ_0, D, and L are respectively 3470 nm, 26.5 ps nm^{-1} km^{-1}, and 4.2 m. By simple calculation, it is concluded that the slope of the least square linear fit of the squared wavelength offset versus sideband order (i.e., the item in the left of Eq. 2) is 7.2×10^{-16}. When we replace $\Delta\lambda_N$ with the wavelength offset of the spikes identified in the spectrum shown in Fig. 4(a), however, it is found that the value of the slope cannot be reached for any possible sideband order. In practice, to reach a slope of 7.2×10^{-16}, the first order sideband should be of an offset from the central wavelength as large as 26.8 nm, which is clearly beyond the distance between the central wavelength and the closest prominent spikes. Therefore, the spikes cannot be simply verified as Kelly sidebands, and the operating regime of the pulse cannot be determined. Figure 4(b) demonstrates the oscilloscope trace of the pulse train. The adjacent pulses are spaced by 39.6 ns. The RF spectrum of the 3.5 μm mode-locked laser is presented in Fig. 4(c), which is acquired with a RBW of 1 kHz. The fundamental frequency (i.e., the repetition rate of the laser) is 25.2 MHz, with a signal-to-noise ratio (SNR) of ~50 dB. The repetition rate is in good agreement with the 39.6 ns space between the adjacent pulses. The pulse energy is calculated to be 0.98 nJ as the 25 mW output power is taken into account. The SNR of the RF beat (~50 dB) is lower than that observed in stable mode-locked fiber lasers (60~80 dB). Thus, the mode-locking appears to be unstable. This is perhaps induced by the environmental factors, given that the system is established in a free-space setup and the ZBLAN fiber is highly sensitive to thermal effects. The RF spectrum in a 500 MHz span is presented in the inset with a RBW of 30 kHz. Owing to the limited bandwidth (250 MHz) of the photodetector, the amplitudes of the harmonics drop rapidly. Unfortunately, the specific pulse duration of the 3.5 μm mode-locked pulse cannot be accurately determined given that the highest power achieved in the experimental works is still below the response threshold of our autocorrelator. The transform limited pulse duration is calculated as 1.66 ps for sech^2 pulse, according to the 7.6 nm FWHM of the spectrum.

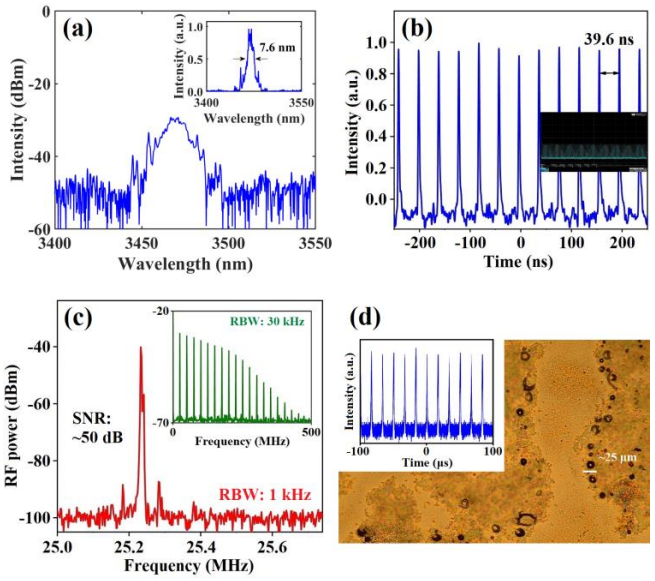

Fig. 4. Characteristics of the 3.5 μm mode-locked pulses: (a) optical spectrum, inset: optical spectrum in linear format; (b) pulse train; (c) RF spectrum around the fundamental frequency, inset: RF spectrum in a 500 MHz span. (d) Damaged surface of SWCNT-SAM, inset: pulse train of the Q-switched pulses.

The laser can maintain fairly stable mode-locking operation for ~15 minutes. However, the mode-locking deteriorates and finally collapses into CW laser in longer operation. Sometimes even the CW laser is terminated. It is found that the deterioration is caused by the thermal

induced bending of the angularly cleaved fiber tip. Although the length of the exposed fiber tip that is outside the fiber holder is only ~2 mm, the heat induced by the coupling loss is still enough to soften the tip and bend it. In order to address the issue, endcap or active cooling of the fiber tip is expected in our future works.

By adjusting the focusing manner (and consequently, the intensity) of the laser beam on the SWCNT-SAM, unstable Q-switched operation is triggered. The switch between the mode-locking and the Q-switching operation can be attributed to the change of the incident intensity of the laser beam [41]. Previously Q-switched operation induced by CNT-based SA has been observed in the 2.8 μm Er-doped ZBLAN fiber laser [37]. The oscilloscope trace of the Q-switched pulse train is presented in the inset of Fig. 4(d). The Q-switched pulses are of very high energy, and will damage the SWCNT-SAM quickly. The damaged surface of the SWCNT-SAM is shown in Fig. 4(d).

5. Conclusions

To conclude, we have demonstrated a mode-locked fiber laser operating at 3.5 μm based upon a SWCNT-SAM. The pulse generated from the laser is of a repetition rate of 25.2 MHz. The maximum average power of the mode-locked pulses is 25 mW, corresponding to a pulse energy of 0.98 nJ. The experimental results reveal that SWCNT can be used as an effective SA for the mode-locking in the 3.5 μm spectral region.

Acknowledgement

This work was supported by National Natural Science Foundation of China (NSFC) (61975136, 61935014, 61775146, 61905151); Guangdong Basic and Applied Basic Research Foundation (2019A1515010699); Shenzhen Science and Technology Project (JCYJ20160520161351540, JCYJ20170817100639177, JCYJ20170302151146995, JCYJ20180305125352956, JCYJ20160328144942069, JCYJ20190808141011530); State Key Laboratory of Information Photonics and Optical Communications (IPOC2019ZZ01); State Key Laboratory of Pulsed Power Laser Technology (Grant SKL2018KF04).

References

1. B. G. Lee, M. A. Belkin, R. Audet, J. MacArthur, L. Diehl, C. Pflügl, and F. Capasso, "Widely tunable single-mode quantum cascade laser source for mid-infrared spectroscopy," Appl. Phys. Lett. 91, 231101 (2007).
2. D. Halmer, S. Thelen, P. Hering, and M. Murtz, "Online monitoring of ethane traces in exhaled breath with a difference frequency generation spectrometer," Appl. Phys. B 85, 437 (2006).
3. C. Frayssinous, V. Fortin, J. P. Berube, A. Fraser, and R. Vallee, "Resonant polymer ablation using a compact 3.44 μm fiber laser," J. Mater. Process Tech. 252, 813 (2018).
4. H. Nie, F. Wang, J. Liu, K. Yang, B. Zhang, and J. He, "Rare-earth ions-doped mid-infrared (2.7–3 μm) bulk lasers: a review," Chin. Opt. Lett. 19(9), 091407 (2021).
5. H. Gu, Z. Qin, G. Xie, T. Hai, P. Yuan, J. Ma, and L. Qian, "Generation of 131 fs mode-locked pulses from 2.8 μm Er:ZBLAN fiber laser," Chin. Opt. Lett. 18(3), 031402 (2020).
6. A. Schliesser, N. Picqué, and T. W. Hänsch, "Mid-infrared frequency combs," Nat. Photonics 6, 440 (2012).
7. H. Uehara, D. Konishi, K. Goya, R. Sahara, M. Murakami, and S. Tokita, "Power scalable 30-W mid-infrared fluoride fiber amplifier," Opt. Lett. 44(19), 4777 (2019).
8. J. F. Li, H. Y. Luo, B. Zhai, R. G. Lu, Z. N. Guo, H. Zhang, and Y. Liu, "Black phosphorus: a two-dimension saturable absorption material for mid-infrared Q-switched and mode-locked fiber lasers," Sci. Rep. 6, 30361 (2016).
9. P. H. Tang, Z. P. Qin, J. Liu, C. J. Zhao, G. Q. Xie, S. C. Wen, and L. J. Qian, "Watt-level passively mode-locked Er^{3+}-doped ZBLAN fiber laser at 2.8 μm," Opt. Lett. 40(21), 4855 (2015).
10. O. Henderson-Sapir, J. Munch, and D. J. Ottaway, "Mid-infrared fiber lasers at and beyond 3.5 μm using dual-wavelength pumping," Opt. Lett. 39(3), 493 (2014).
11. A. Malouf, O. Henderson-Sapir, M. Gorjan, and D. J. Ottaway, "Numerical modeling of 3.5 μm dual-wavelength pumped erbium-doped mid-infrared fiber lasers," IEEE J. Quantum Electron. 52(11), 1600412 (2016).
12. F. Maes, V. Fortin, M. Bernier, and R. Vallee, "5.6 W monolithic fiber laser at 3.55 μm," Opt. Lett. 42(11), 2054 (2017).
13. N. Bawden, H. Matsukuma, O. Henderson-Sapir, E. Klantsataya, S. Tokita, and D. J. Ottaway, "Actively Q-switched dual-wavelength pumped Er^{3+}:ZBLAN fiber laser at 3.47 μm," Opt. Lett. 43(11), 2724 (2018).
14. F. Jobin, V. Fortin, F. Maes, M. Bernier, and R. Vallee, "Gain-switched fiber laser at 3.55 μm," Opt. Lett. 43(8), 1770 (2018).
15. H. Y. Luo, J. Yang, F. Liu, Z. Hu, Y. Xu, F. Yan, H. L. Peng, F. Ouellette, J. F. Li, and Y. Liu, "Watt-level gain-switched fiber laser at 3.46 μm," Opt. Express 27(2), 1367 (2019).
16. O. Henderson-Sapir, N. Bawden, M. R. Majewski, R. I. Woodward, D. J. Ottaway, and S. D. Jackson, "Mode-locked and tunable fiber laser at the 3.5 μm band using frequency-shifted feedback," Opt. Lett. 45(1), 224 (2020).
17. M. Zhang, H. Chen, J. Yin, J. Wang, J. Wang, and P. Yan, "Recent development of saturable absorbers for ultrafast lasers," Chin. Opt. Lett. 19(8), 081405 (2021).
18. K. Wu, X. Zhang, J. Wang, X. Li, and J. Chen, "WS_2 as a saturable absorber for ultrafast photonic applications of mode-locked and Q-switched lasers," Opt. Express 23(9), 11453 (2015).
19. D. Fan, C. Mou, X. Bai, S. Wang, N. Chen, and X. Zeng, "Passively Q-switched erbium-doped fiber laser using evanescent field interaction with gold-nanosphere based saturable absorber," Opt. Express 22(15), 18537 (2014).
20. X. Li, J. Peng, R. Liu, J. Liu, T. Feng, A. Qyyum, C. Gao, M. Xue, and J. Zhang, "Fe_3O_4 nanoparticle-enabled mode-locking in an erbium-doped fiber laser," Frontiers of Optoelectronics 13, 149 (2020).
21. J. Liu, X. Li, Y. Guo, A. Qyyum, Z. Shi, T. Feng, Y. Zhang, C. Jiang, and X. Liu, "Harmonic mode-locking: $SnSe_2$ nanosheets for subpicosecond harmonic mode-locked pulse generation," Small 15(38), 1902811 (2019).
22. T. Feng, D. Zhang, X. Li, A. Qyyum, Z. Shi, J. Lu, P. Guo, Y. Zhang, J. Liu, and Q. Wang, "SnS_2 nanosheets for Er-doped fiber lasers," ACS Appl. Nano Mater. 3(1), 674 (2020).

23. Y. Zhao, P. Guo, X. Li, and Z. Jin, "Ultrafast photonics application of graphdiyne in the optical communication region," Carbon 149, 336 (2019).
24. T. Chai, X. Li, T. Feng, P. Guo, Y. Song, Y. Chen, and H. Zhang, "Few-layer bismuthene for ultrashort pulse generation in a dissipative system based on an evanescent field," Nanoscale 10(37), 17617 (2018).
25. Z. P. Qin, T. Hai, G. Q. Xie, J. G. Ma, P. Yuan, L. J. Qian, L. Li, L. M. Zhao, and D. Y. Shen, "Black phosphorus Q-switched and mode-locked mid-infrared Er:ZBLAN fiber laser at 3.5 μm wavelength," Opt. Express 26(7), 8224 (2018).
26. G. Xie, and Z. Qin, "Mid-infrared ultrafast lasers based on two-dimension materials," in CLEO (Optical Society of America, 2018).
27. R. E. Nahory, M. A. Pollack, W. D. Johnston, and R. L. Barns, "Band gap versus composition and demonstration of Vegard's law for $In_{1-x}Ga_xAs_yP_{1-y}$ lattice matched to InP," Appl. Phys. Lett. 33, 659 (1978).
28. H. Kataura, Y. Kumazawa, Y. Maniwa, I. Umezu, S. Suzuki, Y. Ohtsuka, and Y. Achiba, "Optical properties of single-wall carbon nanotubes," Synthetic Met. 103, 2555 (1999).
29. A. Martinez, and Z. P. Sun, "Nanotube and graphene saturable absorbers for fibre lasers," Nat. Photonics 7, 842 (2013).
30. H. Chu, Y. Li, C. Wang, H. Zhang, and D. Li, "Recent investigations on nonlinear absorption properties of carbon nanotubes," Nanophotonics 9(4), 761 (2020).
31. L. Hou, H. Guo, Y. Wang, J. Sun, Q. Lin, Y. Bai, and J. Bai, "Sub-200 femtosecond dispersion-managed soliton ytterbium-doped fiber laser based on carbon nanotubes saturable absorber," Opt. Express 26(7), 9063 (2018).
32. H. Guo, L. Hou, Y. Wang, J. Sun, Q. Lin, Y. Bai, and J. Bai, "Tunable ytterbium-doped modelocked fiber laser based on single-walled carbon nanotubes," J. Lightwave Technol. 37(10), 2370 (2019).
33. Y. Zhou, J. Lin, X. Zhang, L. Xu, C. Gu, B. Sun, A. Wang, and Q. Zhan, "Self-starting passively modelocked all fiber laser based on carbon nanotubes with radially polarized emission," Photon. Res. 4(6), 327 (2016).
34. K. Y. Lau, P. J. Ker, A. F. Abas, M. T. Alresheedi, and M. A. Mahdi, "Mode-locked fiber laser in the C-band region for dual wavelength ultrashort pulses emission using a carbon nanotube saturable absorber," Chinese Opt. Lett. 17, 051401 (2019).
35. S. Fu, X. Zhu, M. Tong, M. Mollaee, K. Wiersma, K. AlYahyaei, J. Zong, A. Chavez, and N. Peyghambarian, "Ho^{3+}-doped all-fiber laser Q-switched by D-shaped fiber carbon-nanotube saturable absorber," IEEE Photon. Technol. Lett. 31(24), 1960 (2019).
36. W. Chen, Y. Lyu, Q. Li, Z. Kang, H. Zhang, G. Qin, H. Li, and Y. Liu, "Wideband tunable, carbon nanotube mode-locked fiber laser emitting at wavelengths around 3 μm," IEEE Photon. Technol. Lett. 31(11), 869 (2019).
37. C. Wei, Y. J. Lyu, H. X. Shi, Z. Kang, H. Zhang, G. S. Qin, and Y. Liu, "Mid-infrared Q-switched and mode-locked fiber lasers at 2.87 μm based on carbon nanotube," IEEE J. Sel. Top. Quantum Electron. 25(4), 1100206 (2019).
38. M. S. Dresselhaus, G. Dresselhaus, R. Saito, and A. Jorio, "Raman spectroscopy of carbon nanotubes," Phys. Rep. 409(2), 47 (2005).
39. R. Paschotta, and U. Keller, "Passive mode locking with slow saturable absorbers," Appl. Phys. B 73, 653 (2001).
40. M. L. Dennis, and I. N. Duling, "Exerimental study of sideband generation in femtosecond fiber laser," IEEE J. Quantum Electron. 30(6), 1469 (1994).
41. U. Keller, K. J. Weingarten, F. X. Kartner, D. Kopf, B. Braun, I. D. Jung, R. Fluck, C. Honninger, N. Matuschek, and J. Aus der Au, "Semiconductor saturable absorber mirrors (SESAM's) for femtosecond to nanosecond pulse generation in solid-state lasers," IEEE J. Sel. Top. Quantum Electron. 2(3), 435 (1996).